AIP | Journal of Applied Physics

Effective thermal conductivity in thermoelectric materials

Lauryn L. Baranowski, G. Jeffrey Snyder, and Eric S. Toberer

Citation: J. Appl. Phys. **113**, 204904 (2013); doi: 10.1063/1.4807314
View online: http://dx.doi.org/10.1063/1.4807314
View Table of Contents: http://jap.aip.org/resource/1/JAPIAU/v113/i20
Published by the AIP Publishing LLC.

JOURNAL OF APPLIED PHYSICS **113**, 204904 (2013)

Effective thermal conductivity in thermoelectric materials

Lauryn L. Baranowski,[1] G. Jeffrey Snyder,[2] and Eric S. Toberer[3,a)]
[1]*Materials Science, Colorado School of Mines, 1500 Illinois St., Golden, Colorado 80401, USA*
[2]*Materials Science, California Institute of Technology, 1200 California Blvd., Mail Stop 309-81, Pasadena, California 91125, USA*
[3]*Department of Physics, Colorado School of Mines, 1500 Illinois St., Golden, Colorado 80401, USA*

(Received 6 March 2013; accepted 6 May 2013; published online 23 May 2013)

Thermoelectric generators (TEGs) are solid state heat engines that generate electricity from a temperature gradient. Optimizing these devices for maximum power production can be difficult due to the many heat transport mechanisms occurring simultaneously within the TEG. In this paper, we develop a model for heat transport in thermoelectric materials in which an "effective thermal conductivity" (κ_{eff}) encompasses both the one dimensional steady-state Fourier conduction and the heat generation/consumption due to secondary thermoelectric effects. This model is especially powerful in that the value of κ_{eff} does not depend upon the operating conditions of the TEG but rather on the transport properties of the TE materials themselves. We analyze a variety of thermoelectric materials and generator designs using this concept and demonstrate that κ_{eff} predicts the heat fluxes within these devices to 5% of the exact value. © *2013 AIP Publishing LLC*. [http://dx.doi.org/10.1063/1.4807314]

I. INTRODUCTION

Thermoelectric generators (TEGs) are solid state heat engines that generate a voltage in response to a temperature gradient. Due to the lack of moving parts or working fluids, TEGs are ideal for applications that require durability or long lifetimes, or in situations that preclude routine maintenance. Due to the growing need to generate energy by renewable means, TEGs are increasingly being considered for terrestrial energy applications.[1–4] Extracting the maximum possible power from a given temperature gradient requires optimization of the TEG and associated heat exchanger geometries, as well as the TE material properties. Complicating this optimization are the multiple heat transfer mechanisms that occur within a TEG: in addition to standard Fourier conduction, secondary thermoelectric effects must also be considered. In this paper, we develop the concept of an "effective thermal conductivity," which encompasses both the Fourier and thermoelectric heat transport within the device. This concept allows for easy optimization of TEGs and heat exchangers for maximum power production.

A. Thermoelectric materials

When a thermoelectric material is placed within a temperature gradient, the voltage generated is related to the temperature difference by the Seebeck coefficient (α), where $\alpha = V/\Delta T$.[5] The efficiency of a TE material is determined by its figure of merit zT, which is a function of the Seebeck coefficient (α), electrical resistivity (ρ), thermal conductivity (κ), and absolute temperature (T)

$$zT = \frac{\alpha^2 T}{\rho\kappa}. \tag{1}$$

Throughout much of the 20th century, thermoelectric materials exhibited zT values between 0.5 and 0.8, limiting TEGs to low conversion efficiencies. With the advent of nanostructured thermoelectrics and complex bulk materials in the 1990 s, there has been a sharp increase in zT. These high performing materials have led to thermoelectrics being considered for many applications that were previously thought impractical due to low conversion efficiencies.

B. Thermoelectric generators

Practical thermoelectric generators consist of hot and cold side heat exchangers and a thermoelectric module. This module consists of many individual p and n junctions wired in series to increase the total voltage. The general design is shown in Fig. 1(a). For large temperature gradients, multiple materials can be used to maintain a high zT throughout the leg. Depending on how these materials are electrically wired, this results in either segmented or cascaded generators, shown in Figs. 1(b) and 1(c), respectively. The advantages and disadvantages of these designs will be discussed in depth later in this paper.

Like all heat engines, the efficiency (η) of a TEG is ultimately limited by the Carnot efficiency (η_c)

$$\eta_c = \frac{T_h - T_c}{T_h} = \frac{\Delta T_{TE}}{T_h}. \tag{2}$$

The TEG efficiency can be broken into two terms: the limiting Carnot efficiency and the efficiency relative to Carnot called the reduced device efficiency ($\eta_{r,d}$)[6]

$$\eta = \frac{\Delta T_{TE}}{T_h}\eta_{r,d}. \tag{3}$$

In the constant property model (CPM), α, ρ, and κ (and thus z) are approximated as constant with temperature. In this very simplified case, the expression for efficiency becomes[6]

a)etoberer@mines.edu.

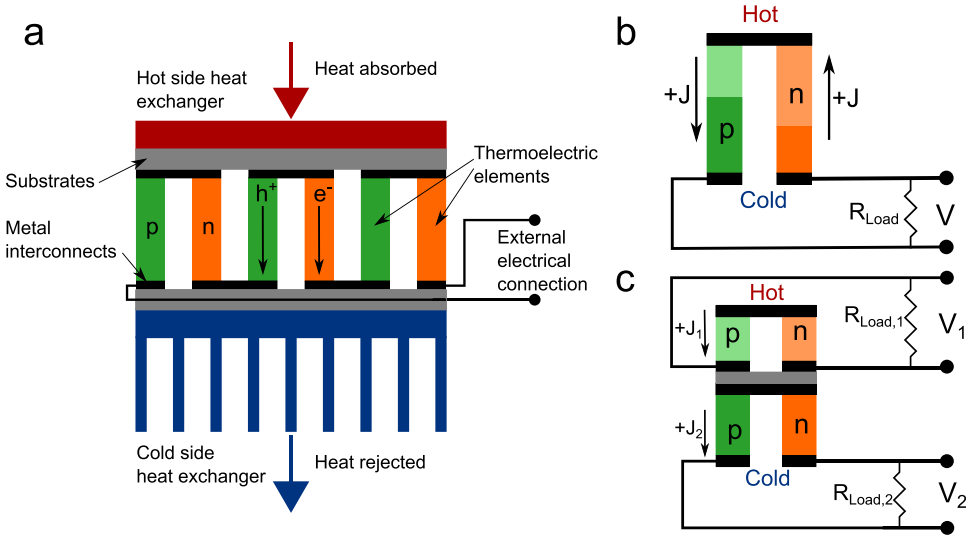

FIG. 1. (a) In a thermoelectric energy harvesting system, many unicouples (n/p pairs) are connected electrically in series to form a module. Heat exchangers are used on either side of the module to enhance heat transfer into/out of the TE module. (b) A segmented module design, in which multiple materials are segmented within each leg to achieve a higher average zT value. (c) A cascaded module design, in which each stage is an independent electrical circuit, allowing for optimization of the current and thermal resistance within each stage.

$$\eta = \frac{\Delta T_{TE}}{T_h}\frac{\sqrt{1+ZT}-1}{\sqrt{1+ZT}+T_c/T_h}. \quad (4)$$

It is important to note that when ZT is used, this denotes an effective device figure of merit, in contrast with zT, the material figure of merit.

While achieving high device efficiency is important, it is often more practical to focus on maximizing the power produced by the TEG, given by

$$P = \eta q_h. \quad (5)$$

We see that the power involves not only the efficiency but also the heat supplied to the TEG (here we denote the heat rate at the hot side of the TEG as q_h).

II. BACKGROUND

There has been a great deal of theoretical work on optimizing η and q_h in a TEG to achieve the maximum power. In the following sections, we review this background work via a thermal circuit model that considers a TEG with heat exchangers on the hot and cold sides. This model allows us to explore system parameters that are important for maximum power production, including thermal resistances and geometric variables.

A. Thermal resistance matching

When designing a TEG and corresponding heat exchangers, the sizing of these components must be carefully considered to achieve maximum power production. The system can be modeled as a thermal circuit, shown in Fig. 2(a). At the hot side, heat (q_h) flows through a heat exchanger with thermal resistance $\Theta_{Hx,h}$ and into the TE module. Because of the Peltier and Thomson effects, there can be significant heat divergence within the TE even at steady state, such that $q_h \neq q_c$. To model this, we use a combination of the thermal resistance Θ_{TE} and a heat sink, such that the heat leaving the TE (q_c) is less than the heat entering the TE (q_h) (for other thermal models, see, for example, Refs. 7–9). Ignoring other heat loss mechanisms, the ratio of these two quantities can be expressed in terms of the efficiency η: $q_c/q_h = 1-\eta$. On the cold side, the heat leaving the TE is then dissipated by a heat exchanger with thermal resistance $\Theta_{Hx,c}$.

The temperature drops across the two heat exchangers can be written as the product of the heat flow and the thermal resistance

$$\Delta T_{Hx,h} = q_h\Theta_{Hx,h}, \quad \Delta T_{Hx,c} = (1-\eta)q_h\Theta_{Hx,c}. \quad (6)$$

These can be summed to give the total temperature drop across the two heat exchangers (ΔT_{Hx}). The combined

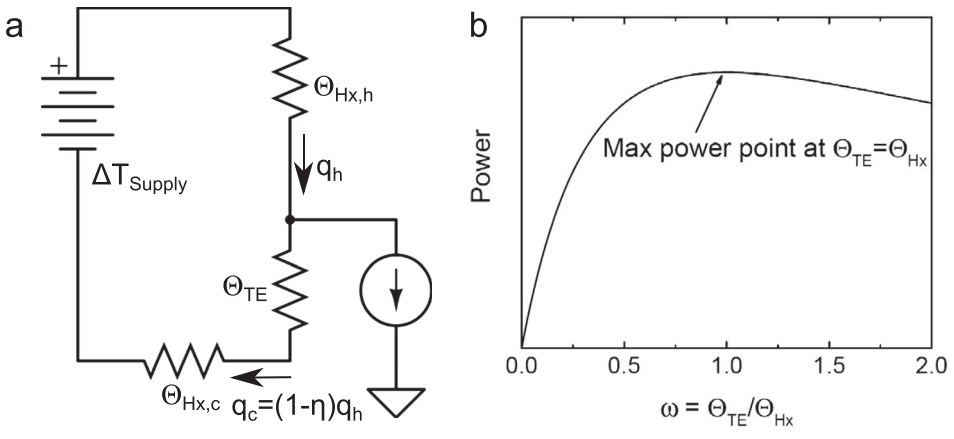

FIG. 2. (a) Equivalent thermal circuit for a thermoelectric energy harvester consisting of hot and cold side heat exchangers and a thermoelectric module. The current source represents the heat generation/consumption due to power production and thermoelectric effects. (b) Variation in power as a function of the ratio of the TE and heat exchanger thermal resistances (Θ_{TE}/Θ_{Hx}). The maximum power point occurs when the two thermal resistances are equal, and significant power losses are incurred when $\Theta_{TE}/\Theta_{Hx} \neq 1$.

thermal resistance Θ_{Hx} is calculated using a weighted sum of the individual heat exchanger thermal resistances

$$\Delta T_{Hx} = q_h(\Theta_{Hx,h} + (1-\eta)\Theta_{Hx,c}) = q_h\Theta_{Hx}. \quad (7)$$

Next, the temperature drop across the TE is related to the heat entering the TE by

$$\Delta T_{TE} = q_h\Theta_{TE}. \quad (8)$$

To examine the effects of ΔT_{Hx} and ΔT_{TE} on the power produced, first recall that the power is given by $P = \eta q_h$. If ΔT_{Hx} is zero, Eq. (7) requires that the value of q_h must be zero, so no power is produced. As ΔT_{Hx} increases, q_h also increases. However, for a constant ΔT_{supply}, increasing ΔT_{Hx} causes ΔT_{TE} to decrease ($\Delta T_{supply} = \Delta T_{Hx} + \Delta T_{TE}$), which decreases the efficiency η. Because the increase of ΔT_{Hx} causes two competing effects, we see that it is important to consider the relative magnitudes of ΔT_{Hx} and ΔT_{TE}. These values are determined by the thermal resistances of the heat exchangers and the TE; it will be shown that the maximum power production is achieved when the two thermal resistances (Θ_{Hx} and Θ_{TE}) are equal.

Using the thermal circuit in Fig. 2(a), the temperature difference across the TE can be expressed as

$$\Delta T_{TE} = \Delta T_{supply}\frac{\Theta_{TE}}{\Theta_{Hx}+\Theta_{TE}}. \quad (9)$$

The total ΔT_{supply} can be written as

$$\Delta T_{supply} = q_h(\Theta_{Hx}+\Theta_{TE}). \quad (10)$$

Substituting Eqs. (3), (9), and (10) into Eq. (5) gives an expression for the power produced

$$P = \frac{\Delta T_{supply}^2\eta_{r,d}}{T_h}\frac{\Theta_{TE}}{(\Theta_{Hx}+\Theta_{TE})^2}. \quad (11)$$

Rather than consider the individual values of Θ_{Hx} and Θ_{TE}, we define the ratio $\omega = \Theta_{TE}/\Theta_{Hx}$. By plotting the power as a function of ω in Fig. 2(b), it is clear that the power is maximized when $\omega = 1$, such that P_{max} is

$$P_{max} = \frac{\Delta T_{supply}^2\eta_{r,d}}{4T_h\Theta_{Hx}}. \quad (12)$$

This result has been demonstrated both numerically and analytically.[10–12]

B. Estimating maximum power production

The maximum power production of the TEG system can easily be estimated using the equations above. Again, because TEG systems are easily scalable, we are concerned with the maximum power flux, rather than the absolute power. This can be expressed by rewriting Eq. (12), recalling that the heat transfer coefficient h_{Hx} is defined as $h_{Hx} = 1/\Theta_{Hx}A_{Hx}$

$$\frac{P_{max}}{A_{Hx}} = \frac{\Delta T_{supply}^2 h_{Hx}\eta_{r,d}}{4T_h}. \quad (13)$$

We now consider the reduced device efficiency of the TEG, $\eta_{r,d}$. Here, we consider two established models to estimate the reduced device efficiency: (1) the constant property model (CPM) and (2) the thermoelectric compatibility model reviewed in the Appendix.

Recall that the CPM defines the material properties α, ρ, and κ as constant, and the reduced efficiency is simply the second term in Eq. (4). In this case, the maximum power is then given by

$$\frac{P_{max}}{A_{Hx}} = \frac{\Delta T_{supply}^2 h_{Hx}}{4T_h}\frac{\sqrt{1+ZT}-1}{\sqrt{1+ZT}+T_c/T_h}. \quad (14)$$

In the CPM, z is constant, and thus zT is a linear function of temperature. In Eq. (14), ZT is used, which must be calculated using an average temperature for the TEG.

By applying the thermoelectric compatibility model detailed in Ref. 6, with the additional assumption of constant zT, the reduced device efficiency can be written as (see derivation in the Appendix)

$$\eta_{r,d} = \frac{2T_h\left(1-\left(\frac{T_c}{T_h}\right)^{\eta_{r,l\max}}\right)}{\Delta T_{supply}}. \quad (15)$$

The maximum local reduced efficiency is a function of the material figure of merit zT

$$\eta_{r,l\max} = \frac{\sqrt{1+zT}-1}{\sqrt{1+zT}+1}. \quad (16)$$

In this model, the expression for the maximum power is then

$$\frac{P_{max}}{A_{Hx}} = \frac{\Delta T_{supply}\, h_{Hx}}{2}\left(1-\left(\frac{T_c}{T_h}\right)^{\eta_{r,l\max}}\right). \quad (17)$$

Both the CPM and the thermoelectric compatibility model provide us with analytic expressions for the maximum power production for a TEG with specific assumptions of material properties (Eqs. (14) and (17), respectively). However, these equations do not tell us how to optimize the system to achieve this maximum power. In Sec. II C, we discuss the geometric optimization of TEGs necessary for maximum power production.

C. Geometric design of TEG systems

In practice, the design of a TEG system normally begins with the choice of heat exchanger. This is because the heat exchangers are likely to be the physically largest components in the system; the thermoelectric module is typically small in comparison. The choice of heat exchanger dictates an approximate heat transfer coefficient $h_{Hx} = 1/\Theta_{Hx}A_{Hx}$: for a forced air heat sink, $h_{Hx} \approx 0.004\,\mathrm{W/cm^2K}$, for a forced water heat exchanger $h_{Hx} \approx 0.6\,\mathrm{W/cm^2K}$.[12]

Once this choice is made, the geometric parameters of the system are considered, recalling that maximum power production requires that $\Theta_{Hx} = \Theta_{TE}$. Because TEG systems are easily scalable, we consider only the ratio of the TE and heat exchanger areas, rather than their absolute values. We

call this ratio the filling factor: $f = A_{TE}/A_{Hx}$. However, the length of the TE leg (l) must still be determined. We can relate this to the heat transfer coefficient as follows:

$$\frac{1}{h_{Hx}} = \Theta_{Hx}A_{Hx} = \Theta_{TE}A_{Hx} = \Theta_{TE}\frac{A_{TE}}{f}. \tag{18}$$

Lastly, we define Θ_{TE} in terms of the effective thermal conductivity of the thermoelectric, κ_{eff}. The concept of effective thermal conductivity is discussed in detail in Sec. III

$$\Theta_{TE} = \frac{l}{\kappa_{\text{eff}}A_{TE}}. \tag{19}$$

This results in a simple equation for the value of l for maximum power production

$$l = \frac{f\,\kappa_{\text{eff}}}{h_{Hx}}. \tag{20}$$

From Eq. (20), we see that the effective thermal conductivity is a powerful concept which enables the design of TEGs for maximum power production. In this paper, we develop an analytic expression for κ_{eff}, with a minimum of assumptions about the material properties of the thermoelectric. This derivation makes use of the thermoelectric compatibility model, rather than CPM; we note that the compatibility model allows straightforward computation of many thermoelectric properties.[13] We then use experimental material property data to determine how closely our expression for κ_{eff} predicts heat transport in real materials. We analyze simple unicouple designs, as well as the more complicated segmented and cascaded TEGs.

III. METHODS

Modeling heat transport within thermoelectric materials requires consideration of not just the Fourier heat conduction but also the Peltier and Thomson effects. Rather than consider each of these effects separately, we derive an "effective thermal conductivity" (κ_{eff}), which allows us to model the entirety of the heat transport in the thermoelectric material using the one dimensional steady-state conduction equation. The final expression for κ_{eff} encompasses not only the traditional Fourier heat conduction but also the heat generation/consumption due to the Peltier and Thomson effects.

In this model, we consider an optimized thermoelectric generator (TEG) using thermoelectric compatibility theory (a brief overview is provided in the Appendix; for a detailed derivation, see Refs. 6 and 14). We assume that the reduced current density (u) is equal to the thermoelectric compatibility factor (s) across the entire TE leg. The $u = s$ condition represents the optimum current density for given values of the temperature gradient and the TE transport properties. Operating at the $u = s$ condition results in the maximum efficiency possible for the given conditions. If the TE element length is allowed to vary, it can be shown that the $u = s$ condition also produces the maximum power possible for the given temperature gradient and transport properties (for a detailed explanation, see section 9.6.4 in Ref. 6). In addition, we assume constant thermal conductivity (κ) and zT. For many TE materials, the κ value varies by less than 50% over a several hundred degree temperature range (see, for example, the κ data in Refs. 15–22). In contrast, the Seebeck coefficient (α) and electrical resistivity (ρ) often vary by an order of magnitude over the same temperature range. Because of this, we do not constrain these values to be constant with temperature. Cascaded and segmented generator designs allow for an approximately constant value of zT. We note that because the $u = s$ model does not inherently assume any material properties, it would be possible to perform an analytic or numerical analysis of κ_{eff} using different assumptions than the ones made here.

The total heat flux (q'') through a TE at any point in the leg can be written in terms of the current density (J) and the thermoelectric potential (Φ) as

$$q'' = J\Phi. \tag{21}$$

This equation includes both the Peltier and the Fourier heat fluxes. We can also write the heat flux in terms of u. Because we are interested in the heat flux into the TE at the hot side (q''_h), we write the reduced form of Eq. (21) specifically for this flux by means of the scaling integral[13]

$$q''_h = \frac{\Phi_h\int_{T_c}^{T_h}\kappa u\,dT}{l}. \tag{22}$$

We wish to express the heat flux in terms of an effective κ that describes the heat flux into the TE at T_h, as defined in Eq. (23). Note that this κ_{eff} will be different than the κ_{eff} derived to describe the q''_c leaving the leg on the cold side

$$q''_h = \frac{\kappa_{\text{eff}}}{l}(T_h - T_c). \tag{23}$$

Equating the two heat fluxes gives an expression for κ_{eff}

$$\kappa_{\text{eff}} = \frac{\Phi_h}{(T_h - T_c)}\int_{T_c}^{T_h}\kappa u\,dT. \tag{24}$$

From Eq. (24), it is clear that we must consider $u(T)$. In order to simplify this task, let $u = s$ across the entire leg. For a thermoelectric generator, in a $u = s$ model,

$$u = s = \frac{\sqrt{1+zT}-1}{\alpha T}. \tag{25}$$

By substituting s into Eq. (24) and recalling that we have defined both κ and zT as constant with temperature, we have

$$\kappa_{\text{eff}} = \frac{\kappa\Phi_h(\sqrt{1+zT}-1)}{T_h - T_c}\int_{T_c}^{T_h}\frac{1}{\alpha T}\,dT. \tag{26}$$

We see that, in order to analytically solve for κ_{eff}, we will need an expression for $\alpha(T)$.

In order to solve for $\alpha(T)$, we first write the heat balance equation in differential form

$$\frac{du}{dT} = u^2T\frac{d\alpha}{dT} + u^3\rho\kappa. \tag{27}$$

Recalling that $z = \frac{\alpha^2}{\rho\kappa}$, this can be rewritten as

$$\frac{\mathrm{d}}{\mathrm{d}T}\left(\frac{-1}{u}\right) = T\frac{\mathrm{d}\alpha}{\mathrm{d}T} + u\frac{\alpha^2}{z}. \tag{28}$$

Also recall that zT is a constant. To simplify, let $zT = k_o$, such that $z = k_o/T$. Substituting our definition of s (see Eq. (25)) into Eq. (28) gives

$$T\frac{\mathrm{d}\alpha}{\mathrm{d}T}\left[\frac{1}{1-\sqrt{1+k_o}} - 1\right] = \alpha\left[\frac{\sqrt{1+k_o}-1}{k_o} - \frac{1}{1-\sqrt{1+k_o}}\right]. \tag{29}$$

To simplify, we define the parameters k_1 and k_2

$$\begin{aligned} k_1 &= \frac{\sqrt{1+k_o}-1}{k_o} - \frac{1}{1-\sqrt{1+k_o}}, \\ k_2 &= \frac{1}{1-\sqrt{1+k_o}} - 1, \\ \frac{k_1}{k_2} &= k_g = \frac{2-2\sqrt{1+k_o}}{k_o}, \end{aligned} \tag{30}$$

such that Eq. (29) becomes

$$\frac{\mathrm{d}\alpha}{\alpha} = k_g\frac{\mathrm{d}T}{T}. \tag{31}$$

This can be solved to give an expression for $\alpha(T)$

$$\alpha = \alpha_{ref}\left(\frac{T}{T_{ref}}\right)^{k_g}. \tag{32}$$

Here, α_{ref} and T_{ref} are simply reference values at any point along the leg.

Substituting our definition of $\alpha(T)$ from Eq. (32) into Eq. (26) and removing constants from the integral gives

$$\kappa_{\mathrm{eff}} = \frac{\kappa\Phi_h\left(\sqrt{1+zT}-1\right)}{T_h - T_c}\frac{T_{ref}^{k_g}}{\alpha_{ref}}\int_{T_c}^{T_h} T^{-(k_g+1)}\,\mathrm{d}T. \tag{33}$$

As k_g is a constant, the integral can be solved to give

$$\kappa_{\mathrm{eff}} = \frac{\kappa\Phi_h\left(\sqrt{1+zT}-1\right)}{T_h - T_c}\frac{T_{ref}^{k_g}}{\alpha_{ref}}\left(\frac{-1}{k_g}\right)\left(T_h^{-k_g} - T_c^{-k_g}\right). \tag{34}$$

We can define Φ_h in terms of the temperature and the material properties

$$\Phi_h = \alpha_h T_h + \frac{1}{u_h}. \tag{35}$$

Again applying Eq. (25) to replace u with s yields

$$\Phi_h = \alpha_h T_h\left(\frac{\sqrt{1+zT}}{\sqrt{1+zT}-1}\right). \tag{36}$$

This expression for Φ_h can be substituted into Eq. (34) to give

$$\kappa_{\mathrm{eff}} = \frac{\kappa\alpha_h T_h\sqrt{1+zT}}{T_h - T_c}\left(\frac{-T_{ref}^{k_g}}{k_g\alpha_{ref}}\right)\left(T_h^{-k_g} - T_c^{-k_g}\right). \tag{37}$$

Lastly, we can evaluate our expression for $\alpha(T)$ (Eq. (32)) at T_h to give α_h. Combining this with Eq. (37) and simplifying gives us a closed form expression that is solely dependent on our constants

$$\begin{aligned} \kappa_{\mathrm{eff}} &= \frac{\kappa T_h\left(1+zT+\sqrt{1+zT}\right)}{2(T_h - T_c)}\left(1 - \left(\frac{T_h}{T_c}\right)^{k_g}\right), \\ k_g &= \frac{2-2\sqrt{1+zT}}{zT}. \end{aligned} \tag{38}$$

IV. RESULTS AND DISCUSSION

The dependence of κ_{eff} on zT and T_h is examined in Fig. 3. For today's materials (zT values typically between 1 and 2), the κ_{eff} value is approximately 50%–100% greater than κ. This demonstrates that the non-Fourier components of the heat transport (Peltier and Thomson effects) are nontrivial in these materials.

Returning to Eq. (20), we can use the value of κ_{eff} to calculate the optimum leg length for a sample unicouple. Fig. 4 shows both the maximum power flux and the leg length as a function of h_{Hx}. Here, we have used experimental property data ($\alpha(T)$, $\rho(T)$, and $\kappa(T)$) for Bi_2Te_3 p- and n-type materials (data from Refs. 19 and 21) to calculate average zT and κ values for each leg.[23] These average values are used to calculate κ_{eff}, and Eqs. (17) and (20) are applied to map out the design space in terms of h_{Hx} (here, $f = 1$). The maximum power production can be dramatically increased by moving to better heat exchangers: a forced air system gives only 0.1 W/cm^2, whereas a forced water system can generate up to 10 W/cm^2. Here, we note that we are only considering the combined heat transfer coefficient, which encompasses both the hot and cold side heat exchangers. The use of this combined value allows for more freedom when choosing hot and cold side heat exchanger designs: the properties of the individual heat exchangers can vary as necessary for the specific system, as long as the combined heat transfer coefficient is maintained at the desired value. The corresponding leg length is shown; this is not a free parameter of

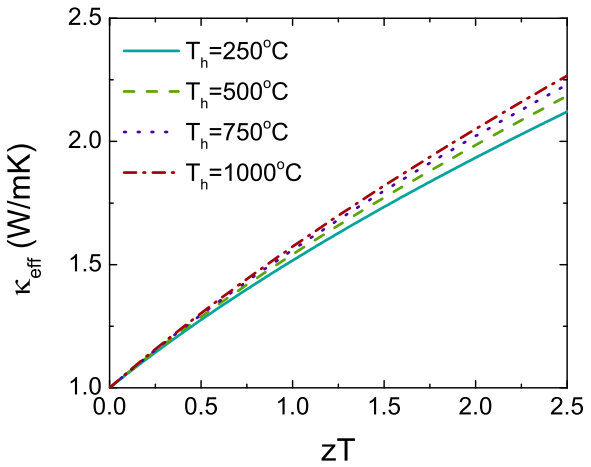

FIG. 3. The variation of κ_{eff} (Eq. (38)) with T_h and zT ($T_c = 25\,^\circ$C, $\kappa = 1$ W/mK). The magnitude of κ_{eff} relative to κ shows that the heat generation/consumption due to the Peltier and Thomson effects is significant.

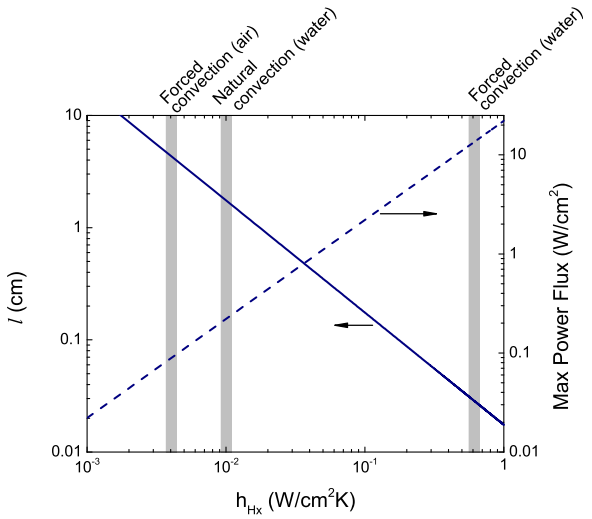

FIG. 4. Estimated maximum power flux and leg length as a function of the combined heat transfer coefficient of the hot and cold side heat exchangers (h_{Hx}) for a Bi_2Te_3 unicouple ($T_c = 25\,^{\circ}C$, $T_h = 250\,^{\circ}C$, $zT = 1.1$). The choice of heat exchanger (h_{Hx} value) greatly affects both the required leg length and the maximum achievable power flux.

the system but rather a constraint imposed by the maximum power condition. In this case, the TE leg length varies between 4.4 cm (forced air) and 0.03 cm (forced water).

A. Performance of κ_{eff} in a unicouple

We can assess the performance of κ_{eff} in predicting real material behavior by considering experimental property data ($\alpha(T), \rho(T)$, and $\kappa(T)$) for p- and n-type Bi_2Te_3 materials between 25 °C and 250 °C (data from Refs. 19 and 21). We use the numerical optimization detailed in Ref. 6 to calculate the exact heat flux into the TE legs (q_h''); this is denoted as q_{ex}''. This is then compared to the heat flux calculated using κ_{eff} according to the equation

$$q_h'' = \frac{\kappa_{\text{eff}}}{l}(T_h - T_c). \tag{39}$$

We call this value $q_{\kappa\,\text{eff}}''$. As a baseline, we also calculate the heat flux as predicted by the standard Fourier conduction equation (Eq. (39)) using an average κ value of the material.

The three heat fluxes are plotted in Fig. 5 as a function of varying hot side temperature. We see very little difference between q_{ex}'' and $q_{\kappa\,\text{eff}}''$, with a maximum absolute difference of 5%. In contrast, the q_{Fourier}'' is significantly different at higher temperatures, with variations up to 35% from q_{ex}''. However, we do note that the divergence between q_{ex}'' and $q_{\kappa\,\text{eff}}''$ becomes larger as the ΔT_{TE} across the TEG increases.

To investigate the behavior of κ_{eff} for larger ΔT_{TE} values, we use data for p- and n-type skutterudite materials to model a unicouple between 50 °C and 525 °C (data from Refs. 16 and 20). The three heat fluxes are calculated as detailed above. In this case, we see even less difference between q_{ex}'' and $q_{\kappa\,\text{eff}}''$, the maximum difference being 2.5%.[23]

These results demonstrate that our κ_{eff} expression is very predictive of the heat transport occurring in TEG

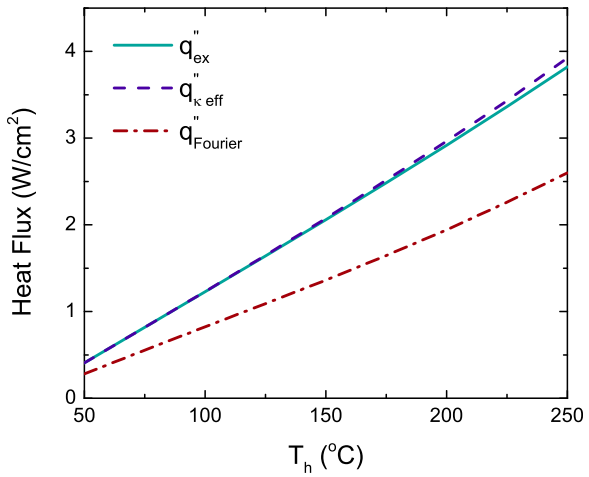

FIG. 5. Heat fluxes calculated using experimental property data (q_{ex}'') and the effective thermal conductivity ($q_{\kappa\,\text{eff}}''$) for a Bi_2Te_3 unicouple with hot side temperatures between 50 °C and 250 °C ($T_c = 25\,^{\circ}C$). For this system, q_{ex}'' and $q_{\kappa\,\text{eff}}''$ differ by less than 5%. In contrast, the heat flux as predicted by Fourier conduction diverges by up to 35%.

unicouples for a range of ΔT_{TE} values. However, unicouple designs are limited in their maximum operating temperatures and efficiencies by the use of a single material. For higher efficiencies, we must look to segmented or cascaded generator designs with large ΔT_{TE} values. In Sec. IV B, we apply the concept of κ_{eff} to these generators.

B. Performance of κ_{eff} in segmented and cascaded designs

The motivation for segmented and cascaded generator designs can be understood using the $u = s$ model. For a $Yb_{14}MnSb_{11}/La_3Te_4$ unicouple between 50 and 1000 °C, the u and s values are close to one another across the legs, but the overall efficiency suffers due to the low zT values of these materials at low temperatures (see Fig. 6). Segmenting several materials within each leg allows for a higher zT value across each leg, giving a higher efficiency. However, u and s are not always within a factor of two of one another, because of the very different s values of the three materials. This problem can be solved by using a cascaded design, in which u can be reset in each stage of the generator. In the cascaded design, the average zT is slightly lower than that of the segmented design, because the electrical isolation of two materials into a stage constrains these materials to an identical temperature range. Regardless, the overall efficiency of the cascaded device is higher because of the better match between u and s in each stage.

To evaluate our expression for κ_{eff} in these systems, we first calculate the κ_{eff} value for each individual material segment in the TEG. Then, thermal circuit models are used to combine the p- and n-type segments/stages into a single value of κ_{eff} for the TEG. For all three of the designs discussed here (large ΔT_{TE} unicouple, segmented, and cascaded generators), the results are very similar to those of the small ΔT unicouple shown in Fig. 5. In all cases, q_{ex}'' and $q_{\kappa\,\text{eff}}''$ values are within 5% of each other. The origins of the success of the κ_{eff} approximation in these complex generators are discussed below.

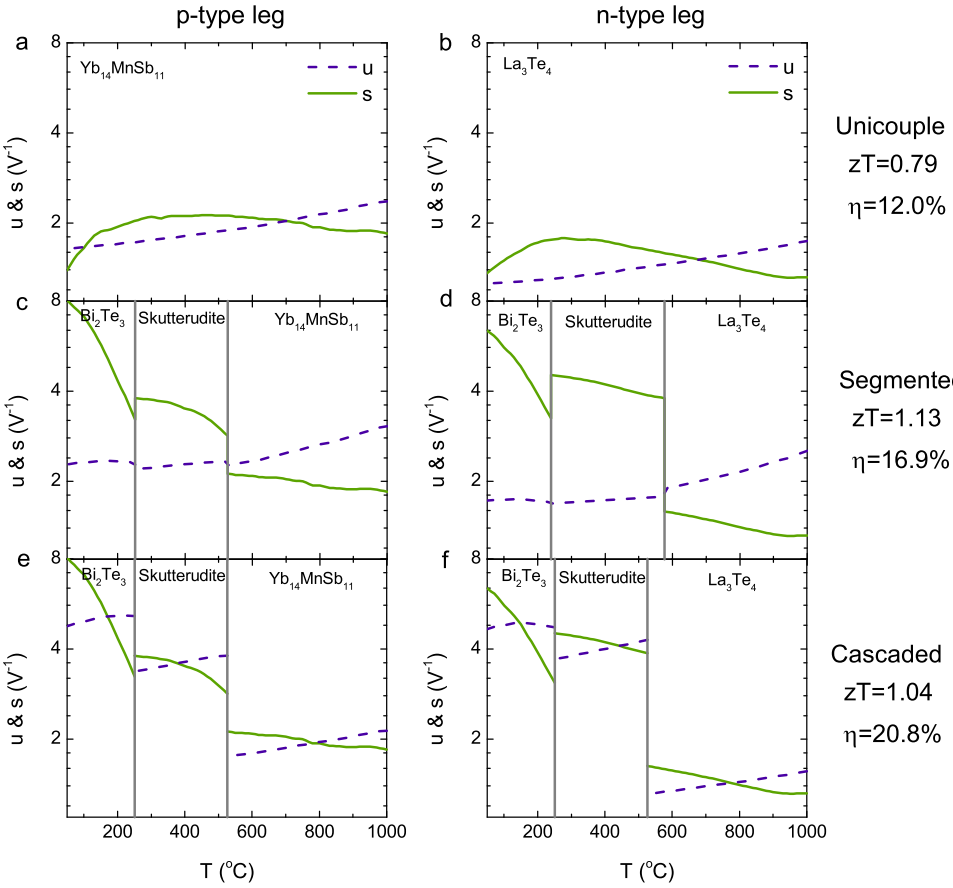

FIG. 6. u and s values for three generator designs with a large ΔT_{TE}. Moving from a unicouple (panels a and b) to a segmented design (panels c and d) increases efficiency because the average zT is higher. The efficiency for a cascaded device (panels e and f) is higher still, because u can be optimized within each individual stage.

C. Further analysis of segmented generators

As can be seen in Figs. 6(c) and 6(d), segmented generators often suffer from a large mismatch between u and s because of the different s values of the materials used. Since the κ_{eff} derived here is based on the $u = s$ assumption, we would expect the heat fluxes predicted using κ_{eff} to be much less accurate in these designs (as compared to a cascaded design with better matching of u and s). However, this is not the case: even in the segmented generator, the difference between q''_{ex} and $q''_{\kappa\,\text{eff}}$ is less than 5%.

The origins of this accuracy can be attributed to the behavior of u and s within the segmented device. From Figs. 6(c) and 6(d), we see that $u > s$ for approximately half the temperature drop across the leg, and $u < s$ over the other half. If the individual values of u and s are averaged across the entire leg, $\bar{u} \approx \bar{s}$. We believe that this averaging effect is important when considering how well κ_{eff} predicts the heat flux for the overall device.

We analyzed data from six different segmented generators (varying temperatures, materials, and number of segments, denoted TEG1-6,[23]), the results of which are shown in Fig. 7. When $\bar{u} > \bar{s}$ (difference between $\bar{s}$ and $\bar{u}$ is negative), κ_{eff} underestimates the heat flux ($q''_{ex} > q''_{\kappa\,\text{eff}}$); the opposite is true when $\bar{u} < \bar{s}$. For the individual segments of the p- and n-type legs (open squares and open circles, respectively), the over/underestimation of the heat flux is considerable. When all the segments in both legs of the TEG are combined,[23] the overall value of κ_{eff} for the generator predicts the heat flux (filled diamonds) within 5% of the exact value. By considering the device as a whole, we are able to extend the accuracy of κ_{eff} past the expected limitations of the model.

V. CONCLUSIONS

We have developed a model for heat transport in thermoelectric materials in which an "effective thermal

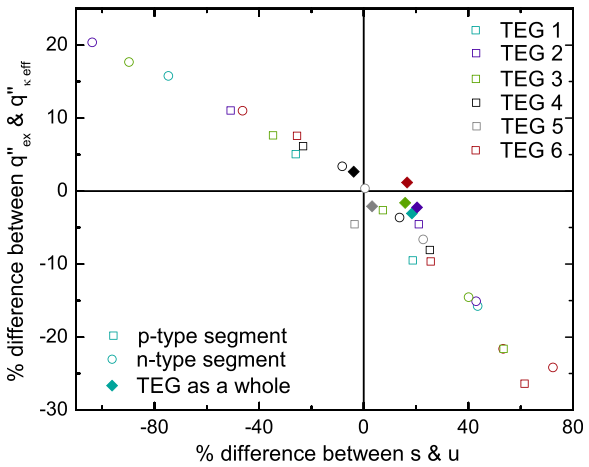

FIG. 7. Heat fluxes calculated for individual segments and segmented generators as a whole; fluxes calculated using κ_{eff} are compared to the exact fluxes (q''_{ex}). Deviations from the ideal $u = s$ model in the individual segments cause large under/overestimations of the heat flux (large differences between $q''_{\kappa\,\text{eff}}$ and q''_{ex}). When the TEG is considered as a whole, the averaging of u and s over the entire device results in a more accurate prediction of the heat flux.

conductivity" encompasses both the one dimensional steady-state Fourier conduction, and the heat generation/consumption due to secondary thermoelectric effects. This expression is especially powerful in that the value of κ_{eff} does not depend upon the operating conditions of the TEG, but rather on the transport properties of the TE materials themselves. Applying the concept of κ_{eff} greatly simplifies thermal analysis of these materials by allowing all of the heat transport to be modeled as Fourier conduction. Through the use of experimental material property data, we have shown that κ_{eff} can accurately predict (within 5%) the heat fluxes for common thermoelectric generator designs.

Although not as accurate as methods such as finite element modeling or the iterative compatibility approach from Ref. 6 (used here as a reference value, q_{ex}), the concept of κ_{eff} allows for simple estimation of the heat fluxes within TEGs with a minimum of computation. This is especially useful when considering the design of TEGs and associated heat exchangers: κ_{eff} can be used to easily determine the design space resulting in maximum power production. There are many other situations in which thermal analysis of TEGs could be simplified using this concept: one such example is the optimization of concentrated solar thermoelectric generators.[4] In addition, the methodology used here could be extended to model Peltier coolers. Because of the generality of this concept, κ_{eff} is a useful tool for the thermal analysis of any thermoelectric material or device.

ACKNOWLEDGMENTS

L.L.B. was supported by the Department of Defense (DoD) through the National Defense Science & Engineering Graduate Fellowship (NDSEG) Program. G.J.S. gratefully acknowledges the Jet Propulsion Laboratory and AFOSR MURI FA9550-10-1-0533 for support. E.S.T. acknowledges the NSF Materials Research Science and Engineering Center at CSM (NSF-MRSEC award DMR0820518) for funding. The information, data, or work presented herein was funded in part by the Advanced Research Projects Agency-Energy (ARPA-E), U.S. Department of Energy, under Award No. DE-AR0000287.

APPENDIX: OVERVIEW OF THERMOELECTRIC COMPATIBILITY THEORY

The efficiency of thermoelectric generators has traditionally been analyzed using the constant property model (CPM), a global approach to the transport properties.[24,25] Recently, a local approach to generator efficiency has been developed which greatly simplifies the analysis and optimization. In addition, this model does not inherently assume any material properties. This approach is derived in Refs. 6 and 13; here, we review the key features.

The macroscopic thermoelectric leg is infinitely divided into layers which are electrically and thermally in series. The maximum local efficiency is set by the local Carnot efficiency dT/T. In practice, the local efficiency is a fraction of dT/T; this fraction is termed the reduced efficiency $\eta_r(T)$. Thus an ideal Carnot generator would have an $\eta_r(T)$ of unity for all T. Given $\eta_r(T)$ across a leg, the global efficiency can be derived

$$\eta_{TE} = 1 - exp\left(-\int_{T_c}^{T_h} \frac{\eta_r}{T}\, dT\right). \tag{A1}$$

We will pursue two approaches, the first with generalized material properties and the second specific to the current state-of-the-art materials. In both cases, prediction of optimum performance requires an optimized reduced current density u. In a thermoelectric leg, the reduced current density can be defined as the ratio of the electric current density, J, to the heat flux by conduction, $\kappa\nabla T$

$$u \equiv \frac{J}{\kappa \nabla T}. \tag{A2}$$

For a constant $\kappa\nabla T$, we can see that u is simply a scaled version of the current density J.

The local reduced efficiency is found to be

$$\eta_r(T) = \frac{u(\alpha - \rho\kappa u)}{u\alpha + \frac{1}{T}}. \tag{A3}$$

By tuning the reduced current density u, η_r can be maximized. The peak in η_r occurs when u is equal to the 'thermoelectric compatibility factor' s, which is defined as

$$s \equiv \frac{\sqrt{1+zT}-1}{\alpha T}. \tag{A4}$$

The maximum reduced efficiency, obtained when $u = s$, is given by

$$\eta_{r,max} = \frac{\sqrt{1+zT}-1}{\sqrt{1+zT}+1}. \tag{A5}$$

As a general rule, $\eta_r(T)$ is significantly compromised when u deviates from s by more than a factor of two. This can be seen in the variation of $\eta_r(T)$ as a function of u in Fig. 8.

To give an analytical expression for the global efficiency, we assume that $u = s$ across the device. Cascading allows u to be reset throughout the legs, enabling a real

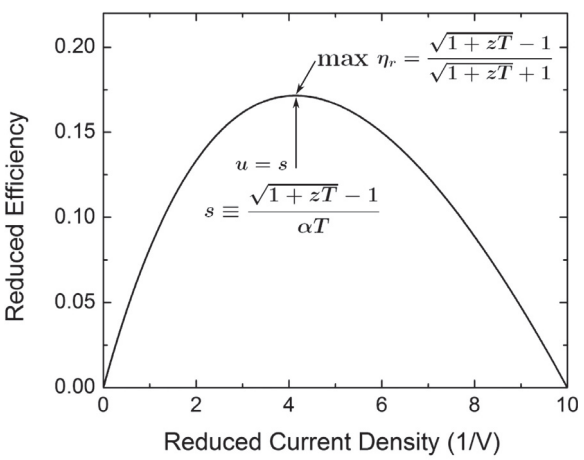

FIG. 8. The variation in reduced efficiency as a function of reduced current density as given by Eq. (A3). The maximum efficiency is achieved when u is equal to the compatibility factor s. For this plot, $zT = 1$, $\alpha T = 0.1$ V, similar to values for Bi_2Te_3.

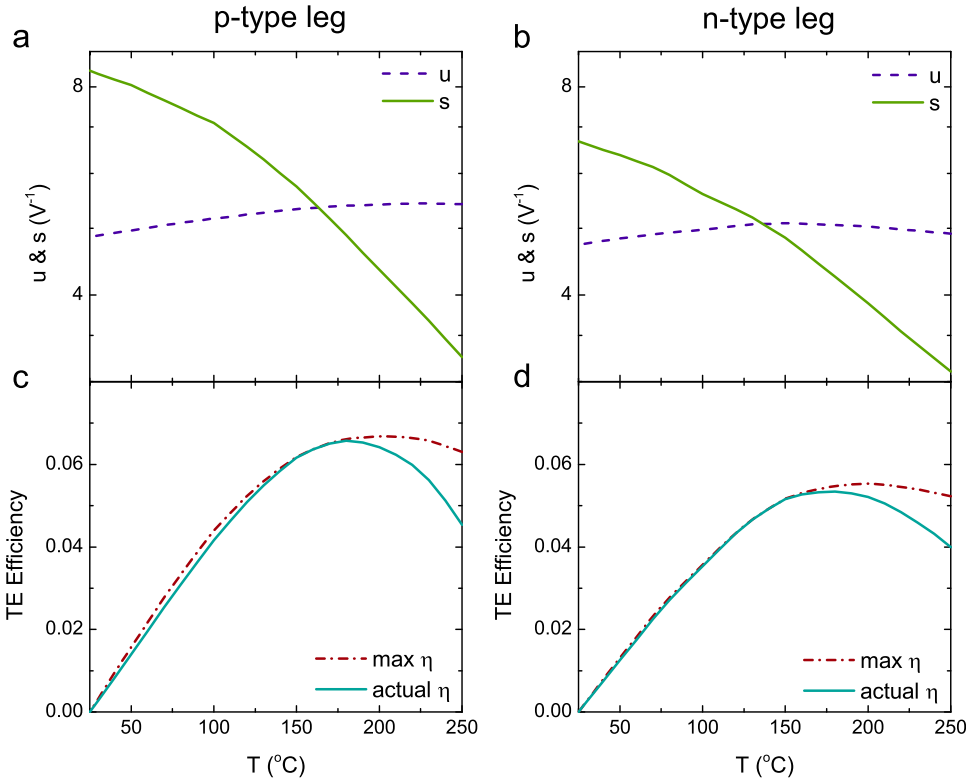

FIG. 9. An optimized TEG using experimental data for p- and n-type Bi_2Te_3 materials. (a) and (b) The reduced current density u is optimized to be as close as possible to the thermoelectric compatibility factor s throughout each leg. (c) and (d) This optimization allows the actual efficiency to be very close to the maximum efficiency, demonstrating that the $u=s$ model is predictive of actual material behavior. Data from Refs. 19 and 21; $T_c=25\,^{\circ}\mathrm{C}$.

device to come close (within a factor of two) to $u=s$ at all T. As can be seen in Eq. (A5), the temperature dependence of zT will be important in evaluating Eq. (A1). In a cascaded generator, the real temperature dependence of zT will have a sawtooth appearance. Here we approximate zT as a constant. If zT is constant, then the reduced efficiency is also constant, and the integral in Eq. (A1) becomes trivial. With these assumptions, the global efficiency can be solved to yield

$$\eta_{TE}=1-\left(\frac{T_c}{T_h}\right)^{\eta_{r,max}}. \tag{A6}$$

A numerical approach can also be used to consider a cascaded STEG constructed from state-of-the-art thermoelectric materials with experimentally determined $\alpha(T)$, $\rho(T)$ and $\kappa(T)$ (and thus $zT(T)$). The interface temperatures between stages are set to maximize zT values. In practice, this typically is the maximum temperature the lower temperature stage can sustain. This approach maximizes η_{TE} for a segment with a given $s(T)$ by iteratively determining the optimum $u(T)$. The efficiency η_{TE} is related to the change in thermoelectric potential (Φ) across the device

$$\eta_{TE}=\frac{\Phi_h-\Phi_c}{\Phi_h}. \tag{A7}$$

The thermoelectric potential is defined as[13]

$$\Phi(T)=\alpha T+\frac{1}{u}. \tag{A8}$$

The heat balance equation can be expressed in reduced form

$$\frac{\mathrm{d}u}{\mathrm{d}T}=u^2T\frac{\mathrm{d}\alpha}{\mathrm{d}T}+u^3\rho\kappa. \tag{A9}$$

This governing expression determines the form of $u(T)$. The boundary condition for $u(T)$ is iteratively determined to maximize the global η.

To consider how well the $u=s$ model predicts actual TE behavior, we use experimental data for $\alpha(T)$, $\rho(T)$, and $\kappa(T)$ for p- and n-type Bi_2Te_3 materials between 25 °C and 250 °C (data from Refs. 19 and 21). The u and s values throughout the p- and n-type legs can be calculated using Eqs. (A4) and (A9). These are plotted in Figs. 9(a) and 9(b). Next, we compare the TE efficiency, which is the product of the reduced and Carnot efficiencies. The maximum efficiency is calculated from Eq. (A5). This is compared to the actual efficiency, given by Eq. (A3), and plotted in Figs. 9(c) and 9(d). In general, actual efficiency is not significantly compromised as long as u and s are within a factor of two of one another.

[1]G. J. Snyder and E. S. Toberer, "Complex thermoelectric materials," Nature Mater. **7**, 105–114 (2008).
[2]E. S. Toberer, L. L. Baranowski, and C. Dames, "Advances in thermal conductivity," Annu. Rev. Mater. Res. **42**, 179–209 (2012).
[3]L. E. Bell, "Cooling, heating, generating power, and recovering waste heat with thermoelectric systems," Science **321**, 1457–1461 (2008).
[4]L. L. Baranowski, G. J. Snyder, and E. S. Toberer, "Concentrated solar thermoelectric generators," Energy Environ. Sci. **5**, 9055–9067 (2012).
[5]T. J. Seebeck, "Magnetische polarisation der Metalle und Erze durch temperatur-differenz," Technical Report, Reports of the Royal Prussian Academy of Science, Berlin, 1823.
[6]G. J. Snyder, *Thermoelectric Power Generation: Efficiency and Compatibility* (CRC Press, Taylor & Francis Group, Boca Raton, FL, USA, 2006), Chap. 9.
[7]S. Lineykin and S. Ben-Yaakov, "Modeling and analysis of thermoelectric modules," IEEE Trans. Indus. Appl. **43**, 505–512 (2007).
[8]M. Chen, L. A. Rosendahl, T. J. Condra, and J. K. Pedersen, "Numerical modeling of thermoelectric generators with varying material properties in a circuit simulator," IEEE Trans. Energy Convers. **24**, 112–124 (2009).
[9]Y. Apertet, H. Ouerdane, O. Glavatskaya, C. Goupil, and P. Lecoeur, "Optimal working conditions for thermoelectric generators with realistic thermal coupling," Europhys. Lett. **97**, 28001 (2012).

[10]J. W. Stevens, "Optimal design of small ΔT thermoelectric generation systems," Energy Convers. Manage. **42**, 709–720 (2001).
[11]Z. Zhou, D. Zhu, Y. Huang, and C. Wang, "Heat sink matching for thermoelectric generator," Adv. Mater. Res. **383–390**, 6122 (2012).
[12]P. M. Mayer and R. J. Ram, "Optimization of heat sink-limited thermoelectric generators," Nanoscale Microscale Thermophys. Eng. **10**, 143–155 (2006).
[13]G. J. Snyder and T. S. Ursell, "Thermoelectric efficiency and compatibility," Phys. Rev. Lett. **91**(14), 148301 (2003).
[14]E. Müller, K. Zabrocki, C. Goupil, G. Snyder, and W. Seifert, "Functionally graded thermoelectric generator and cooler elements," in *CRC Handbook of Thermoelectrics: Thermoelectrics and Its Energy Harvesting*, edited by D. Rowe (CRC Press, Boca Raton, FL, 2012), Vol. 1, Chap. 4.
[15]A. D. LaLonde, Y. Z. Pei, and G. J. Snyder, "Reevaluation of $PbTe_{1-x}I_x$ as high performance n-type thermoelectric material," Energy Environ. Sci. **4**, 2090–2096 (2011).
[16]R. H. Liu *et al*., "p-Type skutterudites $R_xM_yFe_3CoSb_{12}$ (R, M = Ba, Ce, Nd, and Yb): Effectiveness of double-filling for the lattice thermal conductivity reduction," Intermetallics **19**, 1747–1751 (2011).
[17]A. F. May, J. P. Fleurial, and G. J. Snyder, "Optimizing thermoelectric efficiency in $La_{3-x}Te_4$ via Yb substitution," Chem. Mater. **22**, 2995–2999 (2010).
[18]Y. Z. Pei, A. LaLonde, S. Iwanaga, and G. J. Snyder, "High thermoelectric figure of merit in heavy hole dominated PbTe," Energy Environ. Sci. **4**, 2085–2089 (2011).
[19]B. Poudel *et al*., "High-thermoelectric performance of nanostructured bismuth antimony telluride bulk alloys," Science **320**, 634–638 (2008).
[20]X. Shi *et al*., "Multiple-filled skutterudites: High thermoelectric figure of merit through separately optimizing electrical and thermal transports (vol 133, pg 7837, 2011)," J. Am. Chem. Soc. **134**, 2842 (2012).
[21]X. A. Yan *et al*., "Experimental studies on anisotropic thermoelectric properties and structures of n-type $Bi_2Te_{2.7}Se_{0.3}$," Nano Lett. **10**, 3373–3378 (2010).
[22]J. Paik, E. Brandon, T. Caillat, R. Ewell, and J. Fleurial, "Life testing of $Yb_{14}MnSb_{11}$ for high performance thermoelectric couples," in *Proceedings of Nuclear and Emerging Technologies for Space, Albuquerque, NM* (2011).
[23]See supplementary material at http://dx.doi.org/10.1063/1.4807314 for details of these calculations, a plot of these results, details of the generator designs considered, and methods used.
[24]H. J. Goldsmid, *Introduction to Thermoelectricity* (Springer-Verlag, 2010).
[25]R. R. Heikes and R. W. Ure, *Thermoelectricity: Science and Engineering* (Interscience, New York, 1961).